Journal of Electroceramics 3:3, 225–232, 1999


# Magnetic Field and Pressure Effects on the Electrical Resistivity of Single Crystal $Pr_{2/3}(Ca,Pb)_{1/3}MnO_3$

B.A. CLOTHIER, D.Y. JUNG,† P.D. HAN, Z.K. XU & D.A. PAYNE

*Department of Materials Science and Engineering, Science and Technology Center for Superconductivity, and Frederick Seitz Materials Research Laboratory University of Illinois at Urbana-Champaign, Illinois, 61801, USA*

Submitted September 14, 1998; Revised October 22, 1998; Accepted October 23, 1998

**Abstract.** The effects of magnetic field ($H$) and pressure ($P$) on the temperature ($T$) dependence of electrical resistivity ($\rho$) are reported for a new manganese-containing compound, $Pr_{2/3}(Ca,Pb)_{1/3}MnO_3$, which was grown in single-crystal form by a flux method. The material was found to order magnetically with applied-field strength below 175 K, but have zero remanence ($M_R$) as $H \rightarrow 0$, i.e., there was no spontaneous magnetization ($M_S$), only field-induced magnetization ($M_i$). A zero-field ''insulator'' to metal transition occurred at 146 K and this transition temperature ($T_{IM}$) was found to increase with increasing field strength. The change in resistivity with field, $\rho_0 - \rho_H$, normalized with respect to $\rho_H$, was 900% at 146 K and $H = 5\,T$. On application of hydrostatic pressure the zero-field resistivity decreased by 200%/GPa above room temperature. The electrical transport observed was consistent with a thermally-activated process, and this process was found to be relatively independent of pressure (0–4 GPa) in the temperature region (300 K–400 K) studied.

**Keywords:** magnetoresistivity, manganites, pressure, crystal growth, praseodymium

## Introduction

Lanthanide-doped manganites were first reported to exhibit an anomalous peak in the temperature dependence of the electrical resistivity ($\partial\rho/\partial T$) in the 1950s [1,2], and several explanations were initially proposed [3–5]. The anomaly was later found to decrease with increasing magnetic-field strength [6]. The resistivity anomaly and the resulting magnetoresistivity effect have been considered in terms of the role of chemical substitution and bonding on magnetic ordering and electrical transport. Based on the perovskite structure, $ABO_3$, doped manganites are crystalline solutions between $Ln^{3+}Mn^{3+}O_3$ and $M^{2+}Mn^{4+}O_3$, where Ln represents the lanthanide ion (e.g., Pr) and M, the divalent cation (e.g., Ca). Progressive substitution of $M^{2+}$ into the $Ln^{3+}$-site increases the $Mn^{4+}$ content for electronic charge compensation, thereby increasing the acceptor dopant level with holes ($h^\bullet$), i.e., $(Ln^{3+}_{1-x}M^{2+}_x)(Mn^{3+}_{1-x}Mn^{4+}_x)O_3$; $Mn^{3+} + h^\bullet \rightarrow Mn^{4+}$. Therefore, the resulting $Mn^{4+}:Mn^{3+}$ ratio, i.e., $x:(1-x)$, is an important factor for the $p$-type resistivity characteristics of valency-controlled properties [7,8]. The aforementioned temperature dependence of resistivity exhibits a transition between metallic ($\partial\rho/\partial T$ positive) and insulator or semiconductor-like ($\partial\rho/\partial T$ negative) states, at $T_{IM}$. The mixed $Mn^{4+}:Mn^{3+}$ valence states also affect magnetic ordering. The end members, $Ln^{3+}Mn^{3+}O_3$ and $M^{2+}Mn^{4+}O_3$, are commonly antiferromagnets, yet their crystalline solutions, $(Ln^{3+}_{1-x}M^{2+}_x)(Mn^{3+}_{1-x}Mn^{4+}_x)O_3$, display complex magnetic phase relationships [9]. The type of ordering and the temperature onset, $T_C$, are dependent on both chemical substitution and magnetic field strength. In general, the actual value of the electrical resistivity in the ''insulating'' or semiconductor-like state is low and magnetic ordering develops from a paramagnetic ''insulator'' ($T > T_{IM}$) to a ''ferromagnetic'' metal ($T < T_{IM}$) for $0.2 < x < 0.4$. The magnetic transition temperature, $T_C$, is close to $T_{IM}$. Magnetic ordering, electrical transport, and transition temperatures

† Permanent address: Department of Chemistry, Sung Kyun Kwan University, Suwon, Kyunggi-do 440-746, Korea

$(T_C, T_{IM})$ are known to depend on the size, electronic structure and dopant level ($x$) of the A-site cation [9].

A proposed mechanism for the simultaneous observation of electrical conductivity and ferromagnetism with doping in lanthanide manganites was suggested by Zener in terms of a double-exchange model [10]. In the context of this model, the bridging oxygen in the $Mn^{3+}$—O—$Mn^{4+}$ bond can accept or donate electrons, and the exchange energy for the process is favorable if the electron spins are aligned parallel. Above a critical temperature $T_C$, or Curie temperature, a thermally disordered paramagnetic state exists. Below this critical temperature $(T < T_C)$ parallel alignment of electron spins can occur spontaneously (i.e., ferromagnetism) or be induced by an applied field, which leads to a decrease in the magnitude of the resistivity anomaly. It is thought that the double-exchange mechanism alone cannot explain some of the magnetoresistive properties observed in certain manganites. Additional mechanisms may involve a strong electron-phonon coupling believed to arise from Jahn-Teller splitting of the outer $Mn^{3+}$ $d$ energy level [11,12].

However, the double-exchange mechanism does point to the importance of the $Mn^{3+}$—O—$Mn^{4+}$ bond, particularly the bond length and angle, which in turn, can be affected by the size and type of A-site dopant. For example, substitution of larger lanthanide ions or divalent cations, is reported to increase the transition temperatures, $T_{IM}$ and $T_C$, and reduce the magnitude of the magnetoresistivity effect [13]. This has been attributed to ''chemical pressure''. Research has focused primarily on $Ln_{1-x}M_xMnO_3$ derivatives (Ln = La; M = Ca, Sr, Ba, or Pb) in either thin film [14,15] or polycrystalline [16,17] form. Reports on other doped lanthanide manganites (Ln = Pr, Gd, Nd, Sm, etc.) are not as common. Thin-film specimens, while grown with good homogeneity, can suffer from residual stress effects due to lattice mismatch at the film-substrate interface. Such effects could modify the Mn—O—Mn bond length and angle. Polycrystalline specimens, on the other hand, may have chemical heterogeneities and can scatter carriers at grain boundaries. Growth and characterization of high quality $Ln_{1-x}M_xMnO_3$ single crystals would avoid these extrinsic problems, thus allowing for the determination of basic properties. Previous crystals grown, include, $(La_{1-x}Pb_x)MnO_3$ [18], $(Nd_{0.5}Pb_{0.5})MnO_3$ [19], $La_{0.65}(Ca,Pb)_{0.35}MnO_3$ [20], and $Nd_{0.5}(Sr_{0.36}Pb_{0.14})MnO_3$ [21], by $Pb^{2+}$-containing flux methods; and $(La_{1-x}Ca_x)MnO_3$ [22], $(La_{1-x}Sr_x)MnO_3$ [22,23], $(Nd_{1-x}Sr_x)MnO_3$ [24], $(Sm_{0.5}Sr_{0.5})MnO_3$ [25], $(Pr_{1-x}Sr_x)MnO_3$ [26], and $(Pr_{1-x}Ca_x)MnO_3$ [27] by floating zone arc-image methods. In this paper, we report a new $Pr^{3+}$-compound, $Pr_{2/3}(Ca,Pb)_{1/3}MnO_3$, grown in single crystal form by a $Pb^{2+}$-containing flux method, and give experimental data for the effects of magnetic field and external pressure on the temperature dependence of electrical resistivity ($\rho(T,H)$ and $\rho(T,P)$). Previous measurements on these specimens include Raman and optical spectroscopy [28]. Data have also been reported in the literature for polycrystalline specimens of $Pr^{3+}$-containing manganites, including, $Pr_{0.66}(Sr_{0.08}Ca_{0.26})MnO_3$ [29], $Pr_{0.7}(Ba_{0.025}Ca_{0.275})MnO_3$ [29], and $Pr_{0.7}(Sr_{0.05}$-$Ca_{0.25})MnO_3$ [30].

## Experimental Procedure

Crystals of $Pr_{2/3}(Ca,Pb)_{1/3}MnO_3$ were grown from stoichiometric proportions of $Pr_6O_{11}$, CaO, and $MnO_2$ powders, combined with an excess amount of an equimolar mixture of PbO-$PbF_2$ powder, which served as a flux. The proportions corresponded to solute:solvent ratios between 1:10 and 1:5 by weight. The method followed the original approach for $(La_{1-x}Pb_x)MnO_3$ crystals on which the first magnetoresistivity measurements were reported [6,18], and include refinements developed in our laboratory for the growth of ferroelectric $PbTiO_3$ crystals [31]. A similar method was used for the growth of $La_{0.65}(Ca,Pb)_{0.35}MnO_3$. All the chemicals used in the present case were greater than 99.99% purity. The resulting mixture was transferred to an open platinum crucible, which was left unsealed, to allow for sufficient oxidation during thermal processing. The crucible was placed in a vertical, open-air, double-tube furnace, and electrically heated to 1310°C at 100°C/h. After equilibrating for 6 h to ensure complete solubility in the flux, the high-temperature solution was cooled initially at 5°C/h to 1285°C, and then at 2°C/h to 850°C, to induce nucleation, growth, and oxidation. The experiment was terminated by furnace cooling from 850°C to room temperature. There is a possibility of a competing charge-compensation mechanism for acceptor doping which involves oxygen vacancies (□) rather than $Mn^{3+} + h^{\bullet} \rightarrow Mn^{4+}$ valency control. That is,

$Pr^{3+}_{1-x}M^{2+}_{x}[Mn^{3+}]O^{2-}_{3-x/2}\square_{x/2}$ could occur, especially in non-oxidizing environments. In the present case, the experiment was designed to minimize the formation of oxygen vacancies by equilibration and slow cooling in an oxidizing environment. Removal of the crucible from the furnace revealed black cube-like crystals up to 10 mm on an edge. Figure 1 illustrates an as-grown crystal of $Pr_{2/3}(Ca,Pb)_{1/3}MnO_3$. The crystal habit showed a slight elongation in one direction, thus aiding in the identification of the crystallographic $c$-axis. The faces were found to be flat and with well-defined 90° intersections, when observed in an optical microscope.

Powder X-ray diffraction (XRD) of ground single crystals at room temperature provided preliminary information. Analysis of the data gave an orthorhombic structure of the $GdFeO_3$-type with lattice parameters $a = 5.487(1)$ Å, $b = 5.494(1)$ Å, and $c = 7.746(1)$ Å. Reduction to a ''pseudocubic'' perovskite cell parameter $(c_P)$ was accomplished by the transformation $c_P \simeq \sqrt{2}a \simeq \sqrt{2}b \simeq c$ which gave an average length of $c_P \simeq 7.758(1)$ Å and a corresponding angle for $\alpha, \beta, \gamma$ of $\simeq 89.97°$. The slight distortion for the pseudocubic structure is reasonable in light of a ''true'' cubic lattice parameter reported for the derivative compound, $La_{0.65}(Ca,Pb)_{0.35}MnO_3$, of $c = 7.791(1)$ Å [20]. The chemical composition and stoichiometry of selected crystals, estimated before electrical measurements, were carried out by energy dispersive X-ray spectroscopy (EDS), a nondestructive method. A polycrystalline specimen of the stoichiometric composition, $Pr_{2/3}(Ca,Pb)_{1/3}MnO_3$, prepared by solid-state reaction and ceramic processing methods, was used as an EDS standard. After comparison with integrated peak intensity data, the expected $Pr_{2/3}(Ca,Pb)_{1/3}MnO_3$ stoichiometry was confirmed, with a Ca:Pb ratio close to 1:1. Line scans indicated good homogeneity across the surface of the crystals. Later determination by more accurate (but destructive) inductively coupled plasma analysis (ICP) yielded the composition $Pr_{0.63\pm0.01}Ca_{0.18\pm0.01}Pb_{0.19\pm0.01}Mn_{1.00\pm0.02}O_3$. This analysis was carried out after all electrical and magnetic measurements were completed. The average oxidation state of the manganese ion was also determined by iodometric titration on ground single crystal specimens. The oxygen stoichiometery was found to be 3.0 with a standard deviation of $\pm 0.1$.

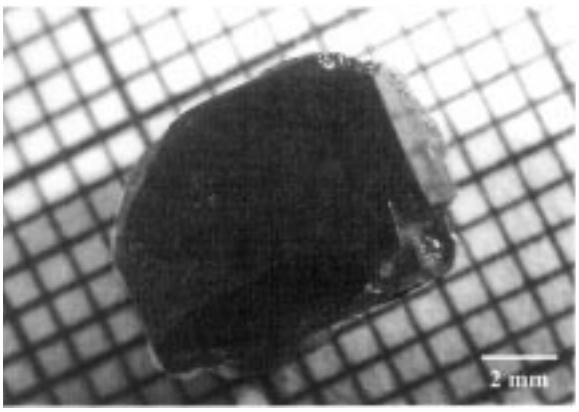


*Fig. 1.* Single crystal $Pr_{2/3}(Ca,Pb)_{1/3}MnO_3$.

Representative crystal specimens were also examined by electron microscopy. A Phillips TEM-420 was used, equipped with a double-tilt cold stage, and operated at 120 kV. The orthorhombic structure was confirmed by convergent-beam electron diffraction patterns, with point group symmetry mmm. Analysis of selected-area electron diffraction patterns gave $a = 5.468$ Å, $b = 5.498$ Å, and $c = 7.702$ Å at 293 K, which are in good agreement with the aforementioned powder-XRD data (which are considered more accurate). EDS data also indicated good chemical homogeneity throughout the TEM specimen. On cooling to 90 K, no change in point group or the formation of any domain patterns was obvious. (Later examination of polycrystalline $(La,Sr)MnO_3$ identified the formation of ferromagnetic domains on cooling for $(La, Sr)MnO_3$, unlike the present case for $Pr_{2/3}(Ca, Pb)_{1/3}MnO_3$[32].)

The effect of magnetic field strength on electrical transport was investigated using a Quantum Design SQUID magnetometer in fields ranging from $H = 0$–$5\,T$ and temperatures from 5–350 K. A standard four-point probe technique was used to determine the resistivity at 1 mA. Since the $c$-axis could usually be identified by inspection, orientation of the specimen along one of the two remaining a and b crystallographic axes was accomplished by Laue X-ray diffraction. Magnetoresistivity measurements were carried out with the current parallel to the magnetic field direction along [100]. $T_{IM}$ was determined as the measurement temperature of maximum resisitivity.

For pressure measurements, a multi-anvil press was used to determine the effect of hydrostatic pressure on electrical resistivity at room temperature and above. Figure 2 illustrates the experimental

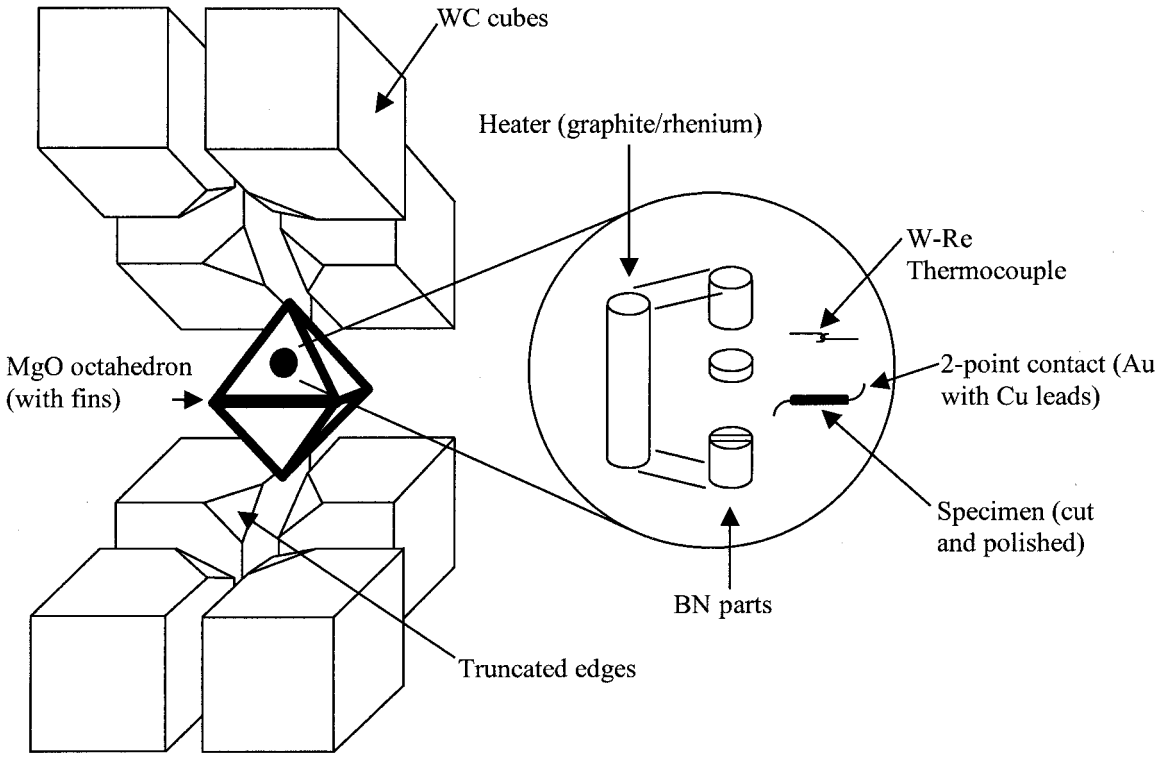


*Fig. 2.* High-pressure and heater assembly.

configuration used. The faces of a $Pr_{2/3}(Ca,Pb)_{1/3}MnO_3$ crystal were cut and polished such that copper leads could be attached along the [100] direction of the crystal via gold contacts. The specimen was then mounted between two boron nitride cylinders one of which contained a rectangular slot. A D-type (W-Re alloy) thermocouple lay just above the specimen, which was isolated by a thin 0.5 mm boron nitride disk. The entire assembly was placed inside a thin-heating sleeve, which in turn, was fitted diagonally inside a hollow octahedral-shaped MgO casting. Pseudo-hydrostatic pressure was applied through corner-truncated tungsten carbide cubes as described elsewhere [33]. The pressure ranged from 0.5 to 4.0 GPa and the temperature from 290 to 525 K. The copper leads formed a two-point probe, which were used to determine the electrical resistivity.

## Results and Discussion

The temperature dependence of magnetization is illustrated in Figure 3 at a field strength of 1 *T*. The figure indicates considerable broadening of the magnetic transition $(M \rightarrow 0)$ which was attributed to induced-magnetization effects. The inset indicates significant deviation from ferromagnetic Curie-Weiss behavior $(\chi = C/(T-\theta), T > T_C)$ with an extrapolated Curie-Weiss temperature $(\theta)$ greater than $T_C$ (175 K). At 1 *T*, $\theta = 210$ K and the Curie constant (C)

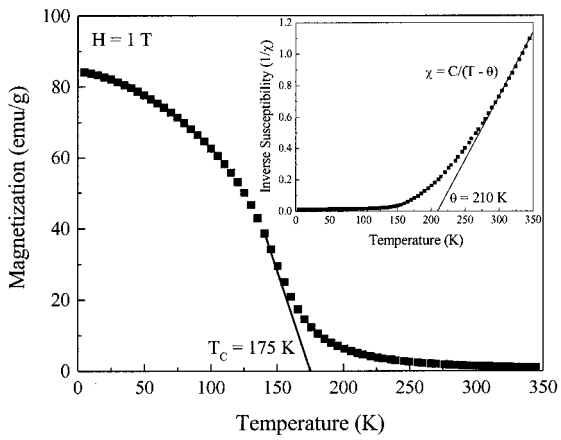


*Fig. 3.* Temperature dependence of magnetization.

was $1.2 \times 10^2$ K. The transition temperature $(T_C)$ of 175 K was interpolated by extrapolation to $M = 0$. Weak field cooling $(H = 10^{-4}\,\mathrm{T})$ indicated the onset of magnetic ordering at 174 K [35], in good agreement with the aforementioned measurements at $H = 1\,T$, but the magnitude of the magnetization at 174 K was four orders of magnitude less $(< 10^{-2}$ emu/g, compare Figures 3 and 4). By comparison with $La_{0.65}(Ca,Pb)_{0.35}MnO_3$ $(T_C = 200\,\mathrm{K})$ the lower transition temperature for $Pr_{0.63}(Ca,Pb)_{0.37}MnO_3$ $(T_C = 175\,\mathrm{K})$ may be correlated with the smaller ionic size of Pr expected from the lanthanide contraction [34]. The effect of magnetic-field strength on properties is further illustrated in Figure 4. For $T \gg T_C$ (e.g., 300 K) linear *M-H* behavior was observed with an effective susceptibility $(\chi = M/H)$ of $\chi = 8.47 \times 10^{-4}$ emu/ cm$^3$. For $T \ll T_C$ (e.g., 5 K), non-linear *M-H* behavior was observed with saturation above 1 *T*. (Note: the thermal demagnetization data reported in Figure 3 was previously measured at 1 *T*.) Figure 4 indicates significant field-induced magnetization effects occurred by 1 *T*, which contributed to the broadening of the magnetic transition in Figure 3. These effects (i.e., temperature dependence of magnetization) will be discussed elsewhere [35]. The field-induced magnetization effects above $T_C$ are reminiscent of field-induced polarization effects in dielectric relaxors and spin-glasses.

Figure 4 also indicates non-hysteretic *M-H* behavior, i.e., the absence of remanent magnetization $(M_R)$ at weak field and $T \ll T_C$. The lack of magnetic hysteresis $(M_R = 0)$ and the immediate response of the induced magnetization $(M_i)$ at weak-field, e.g., $10^{-4}$ T, (with no apparent coercive field $(H_C)$) is more indicative of field-assisted antiferromagnetic-ferromagnetic switching than true ''ferromagnetic'' behavior. The highly susceptible nature at 5 K and weak field gives $\chi = 0.141$ emu/cm$^3$, which is significantly greater $(1.67 \times 10^2$ times) than that at 300 K.

The temperature dependence of resistivity as a function of applied magnetic-field strength $(\rho(T, H))$ is given in Figure 5. These data clearly indicate the resistivity anomaly $\pm(\partial\rho/\partial T)_H$ and the magnetoresistivity effect $-(\partial\rho/\partial H)_T$. The peak resistivity $(\rho_{T_{IM}})$ decreased from 2.89 Ω-cm at zero-field to 0.48 Ω-cm at 5 T (see Fig. 5(a)). Figure 5(b) shows that $T_{IM}$, obtained directly from the measurement

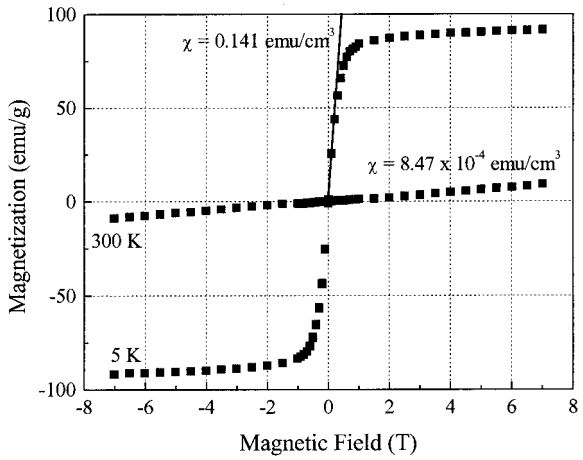


*Fig. 4.* Field-induced magnetization behavior.

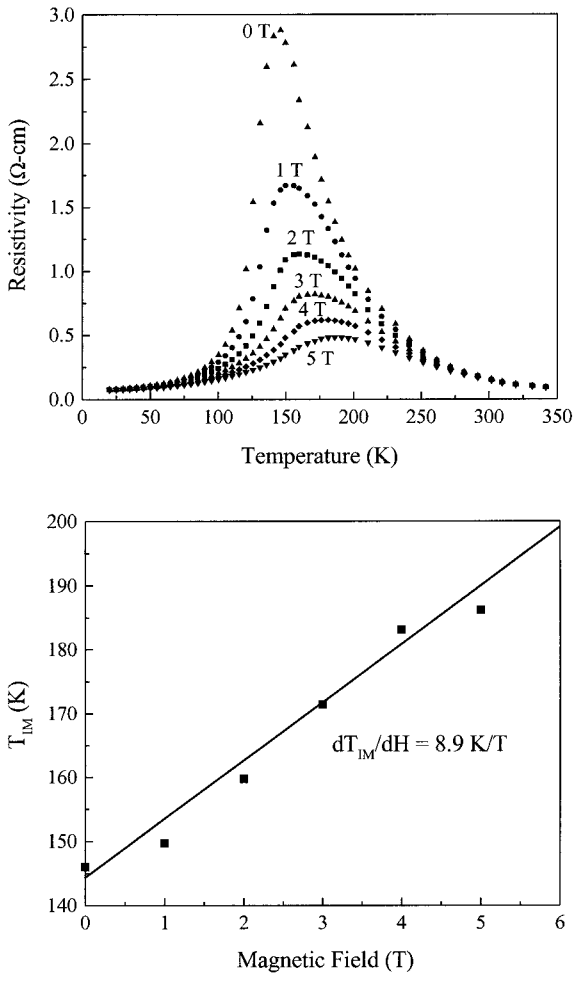


*Fig. 5.* (a) Electrical resistivity along [100] as a function of temperature and magnetic-field strength. (b) Temperature of maximum resistivity, $T_{IM}$, as a function of magnetic-field strength.

temperature for maximum resistivity, increased from 146 to 186 K (i.e., $dT_{IM}/dH = 8.9$ K/T) within the region where the thermal demagnetization temperature occurred ($T_C = 175$ K). On either side of $T_{IM}$, at $T_{IM} \pm 150$ K, the states had equivalent resistivity values of approximately $10^{-1}$ Ω-cm, and the temperature dependence became more symmetrical about $T_{IM}$ at higher field strengths. The actual values of resistivity for $Pr_{0.63}(Ca,Pb)_{0.37}MnO_3$ (i.e., $10^0 - 10^{-1}$ Ω-cm), an orthomanganite with a distorted-perovskite structure, are less than for ferrites (e.g., $(Zn_{1-x}Fe_x)(Mn_xFe_{2-x})O_4$) with the spinel structure (i.e., $\rho = 10^2 - 10^3$Ω-cm) [36] or for other magnetic oxides with the illmenite ($10^6$ Ω-cm) [37], magnetoplumbite ($10^8$ Ω-cm) [38], or garnet structures ($10^{11}$ Ω-cm) [39]. The occurrence of $T_C$ (175 K) within the range for $T_{IM}$ (146–185 K) associates magnetic ordering with the insulator to metal transition and thus the magnetoresistivity effect.

The magnetoresistivity coefficient, Φ, defined as the percentage change in resistivity with applied-field strength at constant temperature (i.e., $\Phi = (\rho_H - \rho_0)/\rho_H \times 100\%$) is given in Fig. 6(a) (from data in Fig. 5(a)). The negative coefficient reaches a maximum value of 900% at 5 $T$ and 145 K (near $T_{IM}$ for $H = 0$). (If normalized with respect to zero-field resistivity ($\rho_0$) the magnetoresistivity coefficient would be $-90\%$.) Note, the large values of Φ are only for an absolute change in resistivity of 2.45 Ω-cm! Figure 6(b) gives the change in temperature ($\sim$ 128–141 K) for the maximum magnetoresistivity ($T_{MR}$) as a function of field strength (0–5 $T$) with ($dT_{MR}/dH$) = 2.5 K/T. The trend is similar to $T_{IM}$ (Fig. 5(b)), and is suggestive of a reduction in carrier scattering due to field-induced alignment of spins. The temperature range for maximum magnetoresistivity (128–141 K) is close to the temperature range for the insulator to metal transition (146–185 K) which depends on applied-field strength.

As stated previously, chemical pressure (attributed to A-site substitution) has been proposed as a possible mechanism for the decrease in resistivity and the increase in transition temperatures observed with increasing ionic size substitution. Similar effects have been reported for applied pressure. For polycrystalline $La_{1-x}Ca_xMnO_3$, hydrostatic pressure (up to 1.7 GPa) was reported to decrease the resistivity and the resistivity anomaly, and increase the zero-field transition temperature, thereby decreasing the magnetoresistivity effect [40]. Similar behavior (up to 1.6 GPa) was reported for single crystal $Nd_{0.5}(Sr_{0.36}Pb_{0.14})MnO_{3-\delta}$ [21]. We have made resistivity measurements up to 5 GPa (Fig. 7). Hydrostatic pressure was found to reduce resistivity at room temperature by approximately 200%/GPa. The pressure dependence of resistivity ($d\rho/dP$) at 300 K and $H = 0$ was $-30$ mΩ-cm/GPa. The progressive decrease in resistivity with applied pressure (Fig. 7(a)) at constant and zero field $(\partial\rho/\partial P)_{H=0}$ was similar to the decrease in resistivity with applied field (Fig. 5(a)) at constant and zero applied pressure $(\partial\rho/\partial H)_{P=0}$. Analysis of the pressure data above room temperature ($T \gg T_{IM}$) gave an activation energy ($E_g$) of 6 meV for $\rho = \rho_0 \exp[-E_g/kT]$ and $T = 300$–400 K; and the activation energy was independent of pressure in the region studied (0–

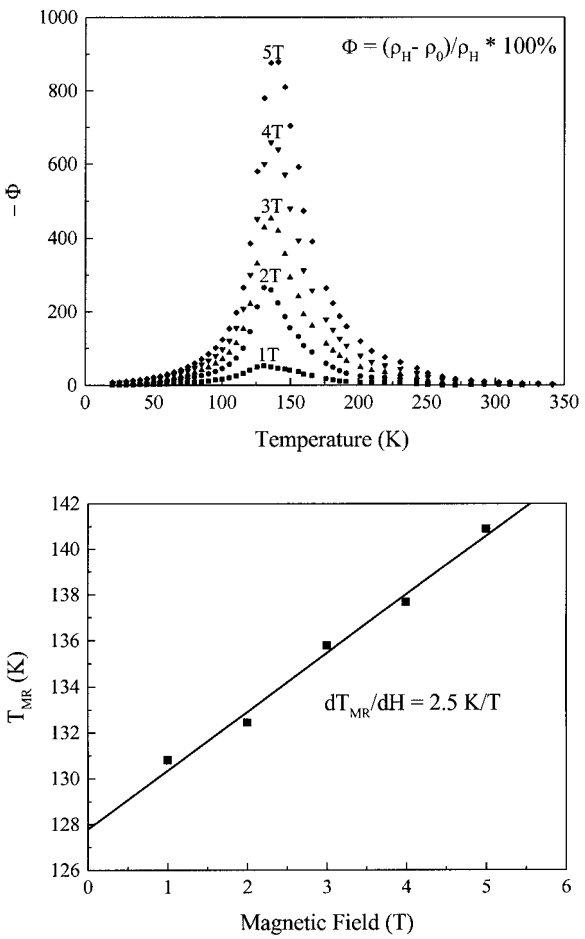


*Fig. 6.* (a) Magnetoresistivity coefficient as a function of temperature. (b) Temperature of maximum magnetoresistivity, $T_{MR}$, as a function of magnetic-field strength.

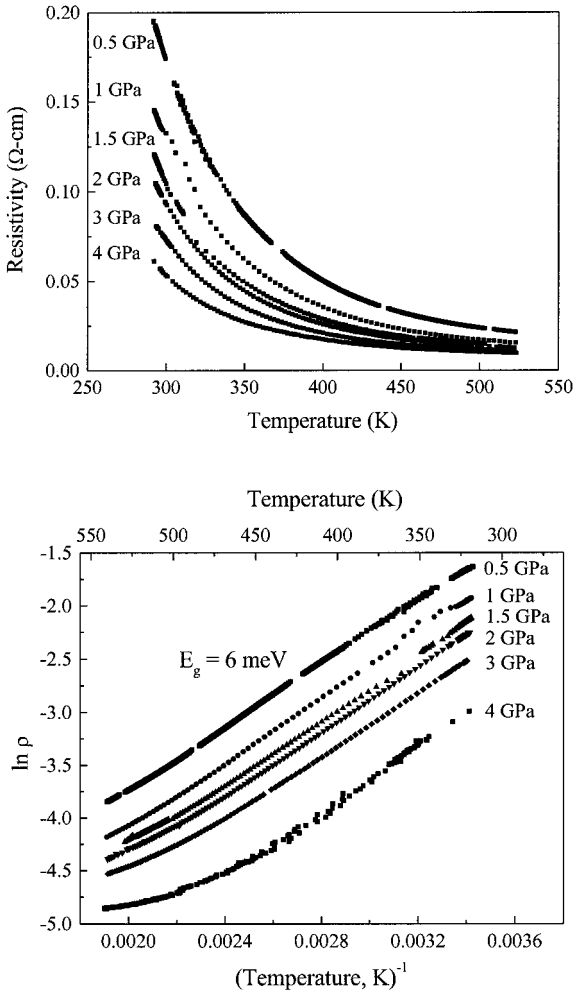


*Fig. 7.* (a) Temperature dependence of resistivity as a function of applied pressure. (b) Thermally-activated transport in the metallic state at constant pressures.

4 GPa). Deviations occurred at temperatures greater than 400 K (Fig. 7(b)). However, in the limited temperature range studied (300–400 K), the results were consistent with thermally activated transport.

A possible explanation is as follows. For valency-controlled semiconductor (semi-insulator) behavior ($Mn^{3+} + h^{\bullet} \rightarrow Mn^{4+}$) the extrinsic carrier concentration $[h^{\bullet}]$ is determined by the dopant concentration $[x]$ and is independent of temperature. Thus, for $T > T_{IM}$, the decrease in resistivity can be associated with an increase in mobility which is thermally activated (6 meV). This would be in accordance with an exchange of carriers between $Mn^{4+}$ and $Mn^{3+}$ sites and could include polaron-hopping type mechanisms. Application of pressure would increase the number of carriers per unit volume (by compressing the lattice) thus leading to a reduction of the resistivity.

Pressure could also lead to a less distorted structure with enhanced bond overlap, increasing the carrier transfer between equivalent manganese sites ($Mn^{3+}$—O—$Mn^{4+}$). Release of the pressure could lead to an increase in resistivity with decreasing temperature. While the nature of electronic structure remains elusive, magnetic ordering of parallel spins occurs with decreasing temperature leading to a compensating process of metallic behavior, i.e., the resistivity passes through an anomaly with decreasing temperature, leading to decreasing resistivity with decreasing temperature. In the vicinity of the anomaly, the decrease in resistivity with increasing magnetic-field strength (i.e., the magnetoresistivity effect) can be attributed to a reduction of carrier scattering by an alignment of magnetic spins.

## Summary

A new compound, $Pr_{2/3}(Ca,Pb)_{1/3}MnO_3$, was grown in single-crystal form by a self-flux method. The structure was orthorhombic mmm at room temperature. The electrical resistivity decreased with increasing pressure ( $\sim$ 200%/GPa) and temperature ($-E_g = 6$ meV). On cooling below room temperature the material exhibited a transition from semiconductor to metallic behavior at 146 K. A field-induced magnetic state occurred below 175 K with zero remanence. No hysteresis behavior was observed. The temperature for the resistivity anomaly increased with increasing magnetic-field strength. At 5 $T$ the magnetoresistivity coefficient was $-900\%$ at 145 K.

## Acknowledgments

The research was supported by the National Science Foundation (DMR 91-20000) through the Science and Technology Center for Superconductivity, and by the U.S. Department of Energy, Division of Materials Sciences (DEFG02-ER9645439), through the Materials Research Laboratory. We are grateful for the use of facilities in the Center for Microanalysis of Materials, and for the technical assistance of David L. West.

## References


1. G.H. Jonker and J.H. Van Santen, *Physica*., **16**, 337 (1950).
2. J.H. Van Santen and G.H. Jonker, *Physica*., **16**, 599 (1950).
3. J.B. Goodenough, *Phys. Rev*., **100**, 564 (1955).
4. P.W. Anderson and H. Hasegawa, *Phys. Rev*., **100**, 675 (1955).
5. P.-G. de Gennes, *Phys. Rev*., **118**, 141 (1960).
6. C.W. Searle and S.T. Wang, *Can. J. Phys*., **48**, 2023 (1970).
7. G.H. Jonker, *Physica*., **20**, 1118 (1954).
8. G.H. Jonker, *Physica*., **22**, 707 (1956).
9. C.N.R. Rao, A.K. Cheetham, and R. Mahesh, *Chem. Mater*., **8**, 2421 (1996).
10. C. Zener, *Phys. Rev*., **82**, 403 (1951).
11. A.J. Millis, P.B. Littlewood, and B.I. Shraiman, *Phys. Rev. Lett*., **74**, 5144 (1995).
12. P. Dai, J. Zhang, H.A. Mook, S.-H. Liou, P.A. Dowben, and E.W. Plummer, *Phys. Rev. B*, **54**, R3694 (1996).
13. R. Mahesh, R. Mahendiran, A.K. Raychaudhuri, and C.N.R. Rao, *J. Solid State Chem*., **120**, 204 (1995).
14. S. Jin, M. McCormack, T.H. Tiefel, and R. Ramesh, *Appl. Phys*., **76**, 6929 (1994).
15. M.F. Hundley, J.J. Neumeier, R.H. Heffner, Q.X. Jia, X.D. Wu, and J.D. Thompson, *J. Appl. Phys*., **79**, 4535 (1996).
16. S. Jin, H.M. O'Bryan, T.H. Tiefel, M. McCormack, and W.W. Rhodes, *Appl. Phys. Lett*., **66**, 382 (1995).
17. G.Q. Gong, C.L. Canedy, G. Xiao, J.Z. Sun, A. Gupta, and W.J. Gallagher, *J. Appl. Phys*., **79**, 4538 (1996).
18. A.H. Morrish, B.J. Evans, J.A. Eaton, and L.K. Leung, *Can. J. Phys*., **47**, 2691 (1969).
19. R.M. Kusters, J. Singleton, D.A. Keen, R. McGreevy, and W. Hayes, *Physica. B*, **155**, 362 (1989).
20. J.Z. Liu, I.C. Chang, S. Irons, P. Klavins, R.N. Shelton, K. Song, and S.R. Wasserman, *Appl. Phys. Lett*., **66**, 3218 (1996).
21. K. Khazeni, Y.X. Jia, Li Lu, V.H. Crespi, M.L. Cohen, and A. Zettl, *Phys. Rev. Lett*., **76**, 295 (1996).
22. T. Hashimoto, N. Ishizawa, N. Mizutani, and M. Kato, *J. Cryst. Growth*, **84**, 207 (1987).
23. A. Urushibara, Y. Moritomo, T. Arima, A. Asamitsu, G. Kido, and Y. Tokura, *Phys. Rev. B*, **51**, 14103 (1995).
24. H. Kuwahara, Y. Tomioka, A. Asamitsu, Y. Moritomo, and Y. Tokura, *Science*, **270**, 961 (1995).
25. H. Kuwahara, Y. Tomioka, Y. Moritomo, A. Asamitsu, M. Kasai, R. Kumai, and Y. Tokura, *Science*, **272**, 80 (1996).
26. Y. Tomioka, A. Asamitsu, Y. Moritomo, H. Kuwahara, and Y. Tokura, *Phys. Rev. Lett*., **74**, 5108 (1995).
27. Y. Tomioka, A. Asamitsu, Y. Moritomo, and Y. Tokura, *Phys. Rev. B*, **53**, R1689 (1996).
28. S. Yoon, H.L. Liu, G. Schollerer, S.L. Cooper, P.D. Han, D.A. Payne, S.-W. Cheong, and Z. Fisk, *Phys. Rev. B*, **58**, 2795 (1998).
29. A. Maignan, C. Simon, V. Caignaert, and B. Raveau, *Comptes Rendus de l'Académie des Sciences*, **321**, 297 (1995).
30. B. Raveau, A. Maignan, and V. Caignaert, *J. Solid State Chem*., **117**, 424 (1995).
31. C.T.A. Suchicital and D.A. Payne, *J. Cryst. Growth*, **104**, 211 (1990).
32. Z. Xu, (private communication).
33. M.H. Frey, Z. Xu, P. Han, and D.A. Payne, *Cer. Trans*., **88**, 169 (1998).
34. B.K. Vainshtein, V.M. Fridkin, and V.L. Indenbom, *Modern Crystallography 2: Structure of Crystals* (Springer-Verlag, Berlin, 1995), p. 74.
35. B.A. Clothier, D.Y. Jung, P.D. Han, and D.A. Payne (to be published).
36. J. Smit and H.P.J Wijn, *Ferrites* (Wiley, New York, 1959), p. 234.
37. G.V. Subba Rao, B.M. Wanklyn, and C.N.R. Rao, *J. Phys. Chem. Solids*, **32**, 345 (1971).
38. J. Baszynski, *Acta. Phys. Pol. A*, **43**, 499 (1973).
39. E.E. Anderson, *J. Appl. Phys. Suppl*., **30**, 299 (1959).
40. J.J. Neumeier, M.F. Hundley, J.D. Thompson, and R.H. Heffner, *Phys. Rev. B*, **52**, R7006 (1995).